CRITICALITY OF DELAMINATION FLAWS IN FIBRE REINFORCED COMPOSITES

James A. Quinn*, Isabel Ward, Colin Robert, Conchúr M. Ó Brádaigh and Edward D. McCarthy
School of Engineering, Institute for Materials and Processes, The University of Edinburgh, UK
* Corresponding author (J.Quinn@ed.ac.uk)

Keywords: flaw criticality, delamination, flexure, compression, damage tolerance

ABSTRACT

This paper presents empirical expressions, which describe the reduction in strength of composites in flexure and compression as a consequence of delamination. A partial factorial study was conducted where the test variable was the laminate thickness (expressed in number of plies), and where delamination flaws were artificially generated at the mid-plane during manufacturing of the specimens using PTFE inserts. The study was conducted for two dissimilar composite systems; a woven glass reinforcement with a polyester resin—typical of composites used in the marine environment, and a pre-impregnated (prepreg) VTC401 epoxy reinforced with unidirectional T700 carbon fibres, which is representative of composites used in the aeronautical/aerospace industry. Specific strength data of artificially delaminated cases were normalised against their reference counterparts to generate normalised specific strength of flawed specimens as a function of laminate thickness. Non-linear fitting of the data has provided asymptotic functions that tend to 1 (the reference value) as ply count (thickness) tends to infinity. From these expressions, users could set optimal bulk material strength reduction design limits which define a critical flaw for their application in terms of the laminate thickness, flaw size, flaw location, and laminate density (linked to fibre volume fraction). Thus, these findings demonstrate the criticality of mid-plane delaminations relative to laminate thickness, and—with the inclusion of further study variables—a full flaw-criticality surface plot can be empirically generated. These results are intended for use in tandem with non-destructive inspection techniques—such as ultrasound—to create quantitative asset maintenance procedures for existing in-service composite structures, particularly where retrofitting structural health monitoring technology is impractical or impossible.

1 INTRODUCTION

An investigation into the effect (criticality) of delamination flaws on the mechanical performance of fibre-reinforced polymer composites is presented. Two types of specimens were manufactured from dissimilar materials: unidirectional carbon fibre epoxy prepreg; and polyester reinforced with woven roving glass mat, such that delaminations were induced in the structure at the interlaminar midplane. Flexural and compression testing exposed the criticality of these flaws—relative to undamaged reference specimens—as a function of laminate total ply count (having five possible values in this study). Furthermore, the relationship between failure modes of composite structures and laminate thickness is explored.

Failure of composite materials has been defined in previous works as the point at which a material is no longer able to satisfy its original design intention [1], which for some structures is the initiation and subsequent propagation of cracks through the structure [1]–[3]. The process of damage propagation to failure can be relatively quick in comparison to structural maintenance intervals. Therefore, it becomes clear that the pre-existence of cracks within composites under new loading conditions (e.g. redeployment of the structure in a new context) might significantly alter the structural load-bearing capacity relative to original design values, potentially causing failure, and consequently, be of vital importance to owners and operators.

Konishi and Lo presented a “screening test” of the criticality of various flaw types in a large partial factorial study of graphite/epoxy composites [4]. Standard tension, compression and bolted-joint tension coupon testing was completed, and the dimensions of a critical flaw were evaluated as those which resulted in fatigue failure of the respective specimens after two lifetimes of accelerated spectrum loading, with two types of ageing factors considered: thermal (varying from -54 °C to 132 °C), and moisture (from dry coupons to coupons with a moisture content of up to 1.29 %). The flaw dimension

factor had up to three additional levels, depending on the load case. Critical flaws were determined to be those with longitudinal fibre termination (holes, scratches). Since this study was only a preliminary report of the partial factorial study, the sample set size was particularly small, at only three specimens per test configuration, so that the results can only indicate general trends. Furthermore, the test matrix includes only in-plane tension and compression testing (and their open-hole test variants), such that the consequence of flaws in situations where interlaminar failure modes are more prevalent, are not accounted for.

A partial factorial experimental program considering interlaminar debonds in graphite epoxy composites was compiled in a technical report to the Naval Air Development Center, Warminster PA, in reference [5] (the first peer-reviewed entry of this work can be found in reference [6]). The factors considered were debond shape (two levels: circular and oblong), and debond size (25.4 mm, 31.75 mm and 38.10 mm in diameter for circular debonds, and 31.75 mm × 25.4 mm and 38.1 mm × 25.4 mm for oblong debonds). Two identical debonds were positioned at the midplane of each 64-ply (layup $[(0_4/\pm 45_2/\mp 45_2/0_4)_s]_s$ totalling approximately 9.7 mm thick), graphite/epoxy specimen during manufacture, located symmetrically with respect to the centre of the specimen span. Specimens were loaded in two separate tests: quasi-static 3-point flexure to failure, and 3-point sinusoidal fatigue loading at 10 Hz with a minimum to maximum stress amplitude ratio of 0.1, and a test duration of 10^6 cycles, with periodic monitoring of flaw propagation. Results for the static element of this study were primarily used to generate stress data to use as inputs for the development of crack propagation models, and to select appropriate load parameters for fatigue testing. As such, no comparison was made with reference specimens (i.e. those without inserted or pre-existing damage prior to testing), and there was limited analysis of results; only that specimens first failed in flexure (tensile failure of outermost off-axis plies), followed by shear failure. The organisation of the noted research acts as good guidance for future works, but given the particular focus on fatigue and its subsequent modelling, the partial factorial approach utilised means that general parametric trends cannot be derived from the data, and as such, the research presents limited advantage for design tasks involving other material systems. Debond position as a design of experiments factor was considered in a subsequent report to the Naval Air Development Centre by the same authors [7]; location, size, shape and sharpness of the debond tips were selected as test factors, having seven, two, two and two levels, respectively.

Given the present lack of studies in the literature, which include laminate thickness as a key variable, this presented research significantly increases understanding of the laminate thickness effect on the criticality of a delamination. While the literature includes partial-factorial studies (containing flaw size, loading conditions, material systems, flaw shape, flaw through-thickness location etc.), no single work yet presents an entire full-factorial flaw criticality study. The present work aims to advance the definition of flaw criticality in generalised terms, in the form of a parameterised model, which contains static flaw size and flaw location over a wide range of laminate thicknesses, for any generic fibrous polymeric composite.

2 EXPERIMENTAL PROCEDURES

2.1 Manufacturing

A partial factorial parametric study was designed to evaluate the consequence of delaminations on the flexure and compression properties of composite materials. Two dissimilar material systems were considered to explore the influence of processing conditions and different reinforcements (in terms of size, weight, orientation etc) on flaw criticality. These were:

1. Type A specimens consisted of 800 g m^{-2} plane woven roving mat manually impregnated with isophthalic polyester resin (Crystic 489PA, with a 2 % (by mass) methylethylketone peroxide (Butanox M50) hardener), consolidated at a pressure of 600 kPa by means of a Radius 70 Tonne platen press. Polyester-glass composite material systems are well established within marine composite contexts, e.g., [8]–[11], and as such, are an ideal candidate for a general study on flaw criticality.

2. Type B specimens were manufactured from pre-impregnated (pre-preg) material consisting of unidirectional carbon fibres (Toray T700, 12k tows) and VTC401 epoxy, by means of a hot-press process using a PEI Pinette heated platen press at 100 °C and 300 kPa. This material system has been comprehensively studied in previous works e.g., [12]–[15], and represents the type of composite typically used in the aerospace industry.

Delaminations were generated in half of the specimens during initial plate manufacturing by insertion of 12.7 µm Teflon PFA film (Lohmann Technologies) at the laminate mid-plane (Fig. 1). The in-plane lengths of each insert, a_1, were determined in reference to the laminate thickness, h, the dimensional ratio of which was constant throughout the test matrix. The delamination in-plane widths, a_2, were equivalent to the specimen widths, b.

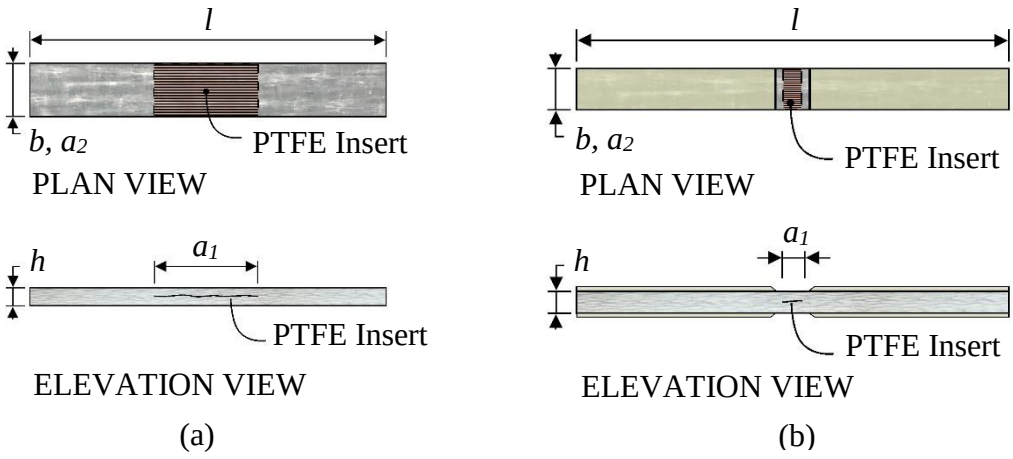

Fig. 1: Schematic of specimens showing flaw position: (a) flexure, (b) compression.

Property	Type A		Type B	
	Flexure	Compression	Flexure	Compression
Number of plies	2, 4, 6, 8, 10	2, 4, 6, 8, 10	4, 6, 8, 10, 12	4, 6, 8, 10, 12
Thickness	h	h	h	h
Width, b (mm)	15.0	13.0	15.0	13.0
Length, l (mm)	20h	140	30h	140
Insert length, a_1 (mm)	2h	10h	6.0	8.0
Insert width, a_2 (mm)	15.0	13.0	15.0	13.0

Table 1: Specimen dimensions.

2.2 Testing

2.2.1 Flexure

Flexure tests were conducted in accordance with ISO 14125 [16], where five specimens per case were loaded in crosshead displacement-controlled flexure at a constant rate using an Instron 3369

benchtop load frame fitted with a 10 kN load cell and Wyoming Test Fixtures Four-Point Flexure Test Fixture. An MTS AVX04 video extensometer package—Allied Vision Manta G-146 camera, Canon EF-S 18-55 mm f/3.5-5.6 IS II lens and MTS AVX software package—was used to capture specimen central displacement data at a sampling rate of 10.02 ± 0.02 Hz, as shown in Fig. 2a. Average specimen widths and thicknesses were calculated from vernier calliper measurements taken at three locations, before a speckle pattern was applied to the central 20 mm of the specimen side (through thickness i.e. the thinnest edge, surface $h \times l$) facing the camera. Specimens were placed centrally on the (5 mm diameter) support rollers with the loading axis being normal to the long edge of the specimen. The extensometer system was set on a tripod and directed at the specimen to observe the specimen speckled region as shown in Fig. 2a. Tests were concluded at ultimate failure of the specimens, defined as an instantaneous stress drop exceeding 50 % of the preceding measured value. Data for time, extension, load, displacement (specimen centre region), and specimen initial cross-sectional area was exported in a csv file for each specimen for analysis using Python 3.

2.2.2 Compression

Compression tests were conducted in accordance with ASTM D6641 [17] where five specimens per case were loaded in crosshead displacement-controlled compression at a constant rate of 1.3 mm/min using MTS Criterion C45.305 electromechanical load frame fitted with a 250 kN load cell and compression platens. A Wyoming Test Fixtures Combined Compression Loading Fixture was used to transfer combined end and shear load from the machine platens to the specimens, as shown Fig. 2b. Linear 1-element strain gauges (FLAB-2-11) were applied to the specimens—in the central gauge region with the measurement axis parallel to the specimen long edge—to capture principal strain data at 1000 Hz. Average specimen widths and thicknesses were calculated from Vernier calliper measurements taken at three locations, before specimens were clamped in the test fixture with the specimen long edge being parallel to the loading axis and clamping pressure applied evenly to the entire tabbed region. Tests were concluded at ultimate failure of the specimens, defined as an instantaneous stress drop exceeding 50 % of the preceding measured value. Data for time, extension, load, principal strain, and specimen initial cross-sectional area was exported in a csv file for each specimen for analysis using Python 3.

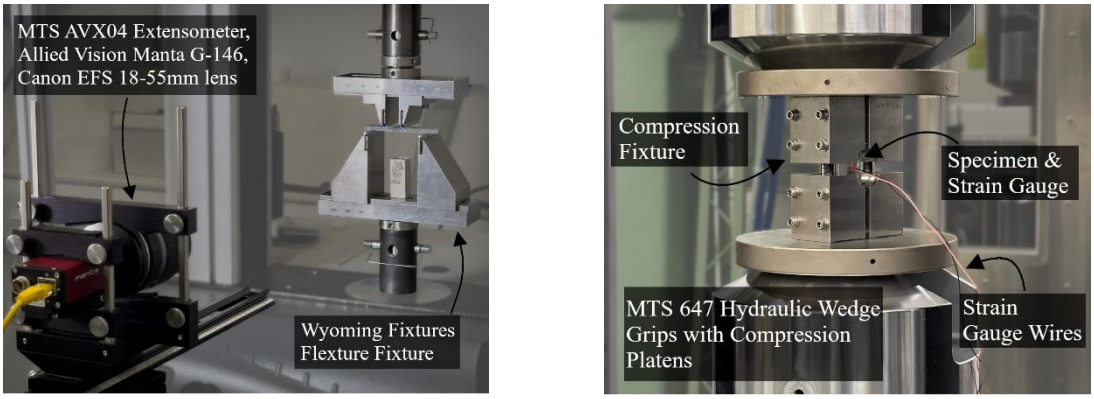

Fig. 2: Labelled photographs of testing setups: (a) flexure, (b) compression.

2.2.3 Density and Fibre Volume Fraction

Density determination was completed using an Ohaus Adventurer AX324 analytical balance paired with an Ohaus density determination kit, which exploits Archemede's principle by comparison of dry mass, A, to that observed when the specimen is submerged in a known liquid, B—shown in Equation 1:

$$\rho_c = \frac{A}{A-B}(\rho_o - \rho_L) + \rho_L \tag{1}$$

where ρ_c is the density of the specimen, ρ_o is the density of the liquid—in this case, distilled water; 0.998 g cm^{-3} at 20 °C—and ρ_L is the air density (0.0012 g cm^{-3}). For each test case, seven extractions approximately equal to 1 cm^3 were cut from random locations in the respective plates using a diamond bladed wet saw. Specimen conditioning before and after submersion was completed in a Prolan Pe70Cl50F40HV benchtop environmental chamber in accordance with ISO 185 291:2008. FVFs, V_r were measured through a pyrolysis/burn-off approach—as specified in ASTM D3171-15 Method I [18]—using a Nabertherm L15/11 muffle furnace and Haldenwanger porcelain crucibles with lids. The expression shown in Equation 2 was used to calculate the FVF where M_r is the mass of reinforcement remaining in the crucible at completion of the pyrolysis. One additional crucible containing traveller fibres verified that fibre mass-loss through the pyrolysis process was negligible.

$$V_r = (M_r) \times 100 \times (\rho_c/\rho_r) \tag{2}$$

3 RESULTS AND DISCUSSION

3.1 Specific and Normalised Properties

To account for possible variations in FVF across cases within the same composite type—for example, the Type A, 2 ply reference case vs. the Type A, 2 ply delaminated case—the absolute strengths observed were converted to specific strengths (σ_{Sf} for flexural strength and X_{SC} for compression strength), by division using the appropriate measured densities, as shown in Equation 3 and Equation 4.

$$\sigma_{Sf} = \frac{\sigma_f}{\rho} \tag{3}$$

$$X_{SC} = \frac{X_C}{\rho} \tag{4}$$

Specific strengths for the delaminated cases (subscripted as "*SC/Sf delaminated case*") were then normalised against their respective reference cases (subscripted as "*SC/Sf reference case*"), as shown in Equation 5 and Equation 6, to create normalised specific strengths for flexure ($\tilde{\sigma}_{Sf}$) and compression ($\tilde{X}_{SC}$).

$$\tilde{\sigma}_{Sf} = \frac{\overline{\sigma_{Sf}}_{delaminated\ case.}}{\overline{\sigma_{Sf}}_{referemce\ case}} \tag{5}$$

$$\tilde{X}_{SC} = \frac{\overline{X}_{SC\ delaminated\ case}}{\overline{X}_{SC\ reference\ case}} \tag{6}$$

The plot for normalised specific strength in compression as a function of laminate ply count, is shown in Fig. 3, and an equivalent plot for flexure is shown in Fig. 4. Non-linear curve fitting of the data was implemented using Python 3, where an asymptotic curve was observed to have good fit, for which the general expression is shown in Equation 7. Asymptotic relationships were selected as the data appears to approach a limiting value of normalised strength for each type. This is reinforced by considering the y = 1 line, which expresses the normalised strength of the respective reference cases. Logically, in the context of the present work, the strength of any specimen having an inserted flaw pre-test should not exceed the strength of a given reference specimen (within the confines of a measurement standard distribution), regardless of the size of a flaw. The parameters α, β and γ for each expression are show in

Table 2. It is speculated that, since the criticality of a given flaw is influenced by many variables that are outside the scope of the present work (flaw size, flaw position through thickness, flaw shape etc.), the parameters α, β and γ will implicitly contain information about these factorials and will be subject to change in line with any of the flaw variables. Exploring this idea further as part of a full factorial study could produce a complete solution to the criticality of any given flaw, which considers all possible flaw variables as inputs.

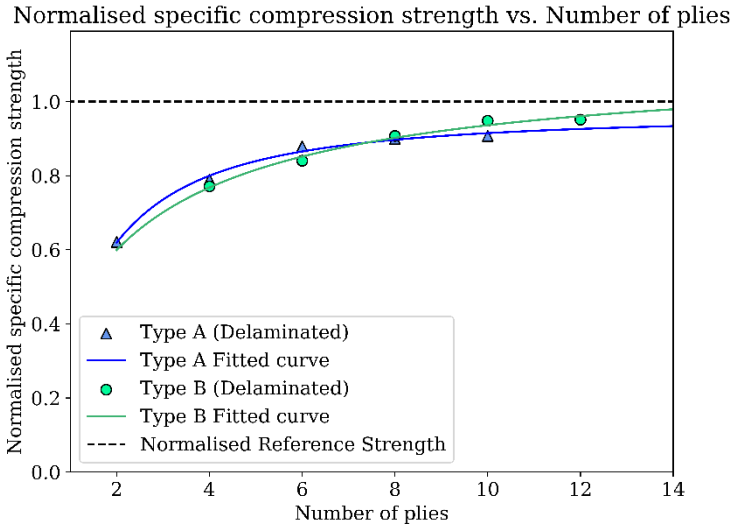

Fig. 3: Normalised specific compressive strength vs. number of plies

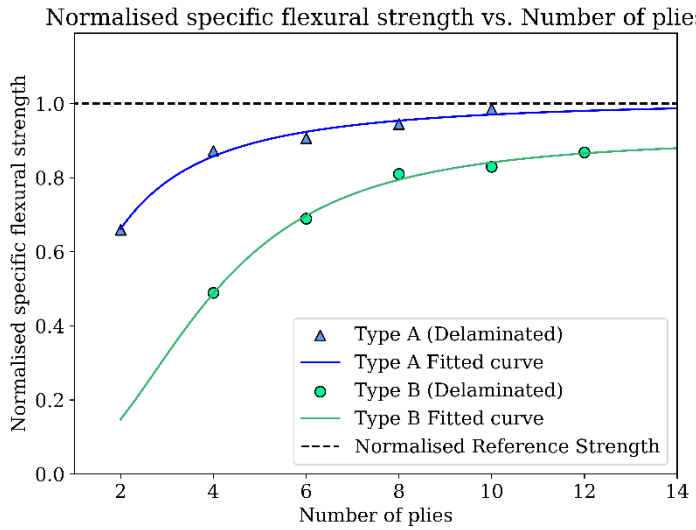

Fig. 4: Normalised specific flexural strength vs. number of plies.

$$\tilde{\sigma}_{Sf} = \frac{\alpha(n.plies^{\beta})}{(n.plies^{\beta})+\gamma} \tag{7}$$

Material System	Flexure α	β	γ	Compression α	β	γ
Type A	1.01	1.55	1.54	0.96	1.51	1.42
Type B	0.91	30.34	2.56	1.12	1.64	0.91

Table 2: Non-linear fitted curve parameters.

3.2 Material Properties and Failure Modes

The raw data was initially processed in accordance with the relevant standards to produce strength and stiffness properties for each test case. Any change in measured material properties can be attributed to the inclusion of a flaw or defect if all other manufacturing and testing variables are reasonably accounted for (e.g., specimen porosity, post curing heat treatment, moisture content etc.). Therefore, material properties for each case were divided by corresponding measured densities to produce specific properties, thereby negating the direct influence of any variations in FVF. The measured, specific mechanical properties of each test case were subsequently normalised against the corresponding specific properties of the relevant reference case, to evaluate the changes in material properties attributed to the inclusion of a mid-plane flaw.

Material System	Ply Count	h (mm)	$\overline{\rho}$ (g cm^{-3})	$\overline{V_r}$ (%)	Reference		Delaminated	
					$\overline{\sigma_f}$ (MPa)	$\overline{X_C}$ (MPa)	$\overline{\sigma_f}$ (MPa)	$\overline{X_C}$ (MPa)
Type A	2	1.3	1.9±0.04	50.3±2.5	564±93	148±23	372±86	92±48
	4	2.2	2.0±0.01	56.8±0.2	532±46	227±26	464±94	179±10
	6	4.4	1.7±0.01	43.2±0.4	430±34	216±49	390±28	190±27
	8	4.7	1.8±0.01	47.5±0.6	338±33	218±29	319±26	196±29
	10	6.6	1.9±0.02	52.5±1.2	357±49	214±16	352±50	194±6
Type B	4	0.8	1.5±0.01	53.4±1.0	1234±74	192±37	604±66	148±38
	6	1.2	1.5±0.01	53.1±1.6	1116±88	231±50	769±45	196±19
	8	1.6	1.5±0.02	52.4±0.8	986±32	206±18	799±54	187±41
	10	2.0	1.5±0.02	52.2±1.3	1131±67	250±12	938±80	237±64
	12	2.4	1.5±0.02	50.2±1.2	1066±86	265±37	926±49	252±35

Table 3: Mean specimen properties as measured in testing.

As can be seen in Table 3, increasing the ply count reduces the mean flexural strength measured in reference specimens during the test, while also (generally) reducing the standard deviation of flexural strength. This could be attributed to the increased probability of crack initiation and propagation sites existing within a larger mass of material. Considering the delaminated specimens, increasing the laminate thickness results in no observed difference in measured flexural strength, since the inserted delamination acts as a primary crack initiation site in all cases. The most common flexural failure mode

in reference specimens was compressive failure of the outermost ply (that which was in contact with the loading pins), which in each test was swiftly followed by a series of interlaminar failures within the side of the specimen under compression. For specimens with embedded delaminations, the failure mode generally shifted towards pure interlaminar failure at the midplane i.e., propagating from the inserted delamination. The inserted delamination overwhelmingly acts as a crack initiation site; thus, a lower quantity of energy is required to grow a crack outward from this insert, when compared to the energy required to induce compressive failure in any of the plies.

Increasing ply count does not significantly alter the compressive strength of the reference laminates, except for generally reducing the standard deviation of measurements. Since the failure in a compression test is generally dominated by the matrix properties—completely unconstrained fibres alone provide negligible compressive strength due to microbuckling—the increased volume of resin in a thicker specimen should cause subsequent increase in probability of a critical crack initiation point existing. When flaws are embedded within compression specimens, the corresponding strengths are reduced by comparison with the reference case, suggesting that the inclusion of the flaw acts as a critical initiation site, from which a critical crack can grow.

Material System	Ply Count	Failure Mode (×quantity observed)	
		Reference	Delaminated
Type A	2	Compressive fracture (×5)	Compressive fracture including interlaminar shear (×5)
	4	Compressive fracture (×5)	Compressive fracture including interlaminar shear (×5)
	6	Compressive fracture (×2) Compressive fracture including interlaminar shear (×3)	Interlaminar shear (×2) Compressive fracture including interlaminar shear (×3)
	8	Compressive fracture including interlaminar shear (×4) Interlaminar shear (×1)	Interlaminar shear (×4) Compressive fracture including interlaminar shear (×1)
	10	Compressive fracture (×2) Compressive fracture including interlaminar shear (×3)	Interlaminar shear (×4) Compressive fracture (×1)
Type B	4	Compressive fracture (×4) Compressive fracture including interlaminar shear (×1)	Interlaminar shear (×3) Compressive fracture including interlaminar shear (×2)
	6	Compressive fracture (×1) Compressive fracture including interlaminar shear (× 4)	Interlaminar shear (×4) Compressive fracture including interlaminar shear (×1)
	8	Compressive fracture (×2) Compressive fracture including interlaminar shear (×3)	Interlaminar shear (×2) Compressive fracture including interlaminar shear (×3)
	10	Compressive fracture (×4) Compressive fracture including interlaminar shear (×1)	Interlaminar shear (×3) Compressive fracture including interlaminar shear (×2)
	12	Compressive fracture (×4) Compressive fracture including interlaminar shear (×1)	Interlaminar shear (×5)

Table 4: Flexural failure modes observed during flexure testing.

4 CONCLUSIONS

An investigation exploring the consequence of delamination flaws on the mechanical properties of fibre-reinforced polymer composites is presented. Two specimen configurations were explored, one representing a typical marine composite, and the other representing a typical aerospace composite. Mid-plane delaminations were induced in the specimens—at one laminate thickness to flaw area aspect ratio—using PTFE sheets, and the specimens were tested in flexure and compression to reveal the criticality of these flaws, compared to undamaged reference specimens. The data reveals asymptotic relationships between flaw criticality and laminate thickness, with flawed specimen strength approaching reference specimen strength as laminate thickness approaches infinity. It is speculated that a full factorial study which includes a range of values for all flaw variables (flaw position, flaw shape, laminate thickness etc.), could enable a series of empirical relationships to be established, which fully describe the criticality of a given flaw within a known material system. That eventuality, when compared with non-destructive testing techniques such as ultrasound, would offer the possibility of increased asset maintenance efficiency and structural safety, as operators could quantitatively estimate the strength of an inspected structure and accurately plan for necessary out-of-service repairs.

ACKNOWLEDGEMENTS

This research was funded in part by the Scottish Research Partnership in Engineering, in collaboration with The University of Edinburgh and Babcock International PLC. All funding sources are hereby gratefully acknowledged.

REFERENCES

[1] E. J. Barbero, “Chapter 7. Strength,” in *Introduction to Composite Materials Design*, Third Edit., Boca Raton: Taylor & Francis, CRC Press, 2017, pp. 227–278.

[2] European Union Aviation Safety Agency, “CS 25.571 Damage tolerance and fatigue evaluation of structure,” in *Certification Specifications and Acceptable Means of Compliance for Large Aeroplanes (CS-25)*, 2021, pp. 264–301.

[3] R. B. Heselhurst, “Chapter 4 Failure Mechanisms,” in *Defects and Damage in Composite Materials and Structures*, First., Boca Raton: Taylor & Francis, CRC Press, 2014, pp. 79–102.

[4] D. Y. Konishi and K. H. Lo, “Flaw Criticality of Graphite/Epoxy Structures,” in *Nondestructive Evaluation and Flaw Criticality for Composite Materials, Philadelphia, Pa.*, 1978.

[5] S. N. Chatterjee and R. B. Pipes, “Study of Graphite/Epoxy Composites for Material Flaw Criticality,” 1980.

[6] S. N. Chatterjee, R. B. Pipes, and R. A. J. Blake, “Criticality of Disbonds in Laminated Composites,” in *Effects of Defects in Composite Materials, ASTM STP 836, American Society for Testing and Materials*, 1984.

[7] S. N. Chatterjee and R. B. Pipes, “Composite Defect Significance,” 1982.

[8] J. Summerscales, “2 - Composites manufacturing for marine structures,” in *Marine Applications of Advanced Fibre-Reinforced Composites*, J. Graham-Jones and J. Summerscales, Eds. Woodhead Publishing, 2016, pp. 19–55.

[9] V. Sánchez-Gálvez, D. A. Cendón, R. Sancho, and F. Gálvez, “Recent Developments on Ballistic Performance of Composite Materials of Naval Relevance,” in *Advances in Thick Section Composite and Sandwich Structures: An Anthology of ONR-sponsored Research*, S. W. Lee, Ed. Cham: Springer International Publishing, 2020, pp. 169–185.

[10] C. Berggreen and B. Hayman, "Damage Tolerance Assessment of Naval Sandwich Structures with Face-Core Debonds," in *Advances in Thick Section Composite and Sandwich Structures: An Anthology of ONR-sponsored Research*, S. W. Lee, Ed. Cham: Springer International Publishing, 2020, pp. 439–483.

[11] S. Sugiman, M. H. Gozali, and P. D. Setyawan, "Hygrothermal effects of glass fiber reinforced unsaturated polyester resin composites aged in steady and fluctuating conditions," *Adv. Compos. Mater.*, vol. 28, no. 1, pp. 87–102, 2019.

[12] E. J. Pappa, J. A. Quinn, J. J. Murray, J. R. Davidson, C. M. Ó Brádaigh, and E. D. McCarthy, "Experimental study on the interlaminar fracture properties of carbon fibre reinforced polymer composites with a single embedded toughened film," *Polymers (Basel).*, vol. 13, no. 23, 2021.

[13] E. Pappa, E. McCarthy, and C. O Brádaigh, "Optimisation of carbon fibre reinforced polymer composites with a thin embedded polyurethane film: Twenty-second International Conference on Composite Materials (ICCM22)," in *Proceedings of Twenty-Second International Conference on Composite Materials (ICCM22), Melbourne, Australia*, 2019.

[14] R. Kok, F. Martinez-Hergueta, and F. Teixeira-Dias, "Tensile response of AP-PLY composites: A multiscale experimental and numerical study," *Compos. Part A Appl. Sci. Manuf.*, vol. 159, p. 106989, 2022.

[15] A. Alsaadi, Y. Shi, and Y. Jia, "Delamination Detection via Reconstructed Frequency Response Function of Composite Structures," in *Proceedings of the 13th International Conference on Damage Assessment of Structures*, 2020, pp. 837–843.

[16] International Organization for Standardization, "BS EN ISO 14125:1998+A1:2011 Fibre-reinforced plastic composites — Determination of flexural properties." BSI Electronic Catalogue, p. 24, 1998.

[17] ASTM, "D6641: Standard Test Method for Compressive Properties of Polymer Matrix Composite Materials Using a Combined Loading Compression (CLC) Test Fixture," pp. 1–13, 2014.

[18] ASTM, "Standard Test Methods for Constituent Content of Composite Prepreg 1," vol. 97, no. December, pp. 1–6, 2010.